

# Minimization by FEM of the transient electrical contact resistance and contact temperature of power automotive connector

Amine BELOUFA

**Abstract**—The purpose of this paper is to analyse and optimize by the finite element code the temperature, the electrical contact resistance and the mechanical stress of power automotive connector submitted to high electric current and high contact forces. High current leads to increase contact temperature due to the generation of the Joule heat and can produce metallurgical changes such as softening or even melting of the conducting areas. This requires the minimization of electrical contact resistance and contact temperature. A finite element model with indirect coupling method of mechanical and thermo-electrical fields and with taken into account the plasticity of the material was developed using a commercial code in order to compute the transient numerical values of contact resistance and contact temperature of contact sample with one contact point. The contact sample was made with recent high-copper alloy C19210 which presents good mechanical, thermal and electrical properties. Another finite element model with multipoint contacts was developed in order to minimize electrical contact resistance and contact temperature. Results showed that contact temperature and electrical contact resistance vary exponentially and increase over time until the equilibrium state. Results showed also the obtaining of triple gains for the model with multipoint contacts: minimization of contact resistance, contact temperature and maximum Von Mises stress which is more interesting for the connector designers.

**Keywords**— Design Optimization, Electrical Contact Resistance, Temperature, Transient Finite Element.

## I. INTRODUCTION

IN last years, several electrical systems are installed in modern cars in order to satisfy the needs of comfort, security, performance and to reduce the fuel consumption. Consequently, the demand in electrical power increases. For example, the necessary electrical power for the hybrid car is higher than 10 kW, while for the electric car is near to 60 kW. To satisfy this growing demand for electrical power in modern car generations, the 14 V battery has to be extended to 42 V. Because of the difficulties of implementing a new 42 V system, the present tendency is to increase current levels at 14 V up to 100 A. This fort current is the origin of the intense

Joule heating in the contact surface of the connector and can contribute to many problems such as softening or even melting of the conducting areas [1], which requires the conception of new power connectors and minimization of electrical contact resistance and contact temperature for the high currents. Moreover, high currents need lower electrical contact resistance  $R_C < 1 \text{ m}\Omega$ . Therefore, the objective of this study is to carry out using the finite element software the numerical minimization of contact resistance, contact temperature and mechanical stress of contact sample with sphere/plane contact geometry and under indentation loading. The sphere/plane contact geometry represents the contact in real connector. The study of electrical contact resistance under indentation, insertion and fretting tests for contact samples made of many recent high-copper alloys has been investigated by Beloufa in many papers [2]-[4]. Beloufa has shown that the material which presents the minimum electrical contact resistance is the copper alloy C19210. For this reason, the material used in our study is the copper alloy C19210. In order to minimize electrical contact resistance and contact temperature, a finite element models with one contact point and five contact points were developed with the help of commercial code Ansys [5], basing to the indirect coupling method with the mechanical and thermo-electrical fields. Much work has been carried out to study the optimisation of shape and strain-stress of different mechanical structures using the finite element method. Reference [6] has optimized by FEM analysis the weight of car rim. It has calculated the equivalent stresses within the rim body for different thicknesses utilizing an elasto-plastic law in order to select the low thickness with a maximum equivalent stress lower than the yield stress. An integrated approach for three dimensional 3D shape optimal design using  $\beta$ -spline surface representation, genetic algorithms and mesh parameterization has been presented in [7]-[10]. Various papers have been devoted to study the optimization of shape and mechanical stress of structure with taken into account the contact conditions [11]-[13] and in the case of structure associated with mechanical, electrical and thermal fields [14]-[16]. However, to the best of the author knowledge, there is no paper in the open literature on the minimization of contact resistance, contact temperature and mechanical stress without changing the weight of contact samples. So, the present paper attempts to fill this gap.

Manuscript received September 27, 2010.

A. Beloufa is with the Prisme Institute, EA 4229, ENSI de Bourges, France. phone: +33615623455; fax:+33248484050; e-mail: beloufaamine@yahoo.fr

## II. CONTACT GEOMETRY

The U-shaped samples (Fig. 1) were made with a sheet of 20 mm in width, using the stamping and bending processing technique. The two parts of the sample (plane part or lower part and the sphere part or upper part with one contact point and with five contact points) are of the same thickness, i.e.  $e = 0.7$  mm. The radius of the sphere segment of each contact point is  $r = 3.6$  mm (Fig. 1). It has been demonstrated by [17] that the contact resistance for sphere/plane contact was lower than that for the cylindrical/plane contact. Therefore, the U-shaped samples used in our study have a contact shape with a spherical segment.

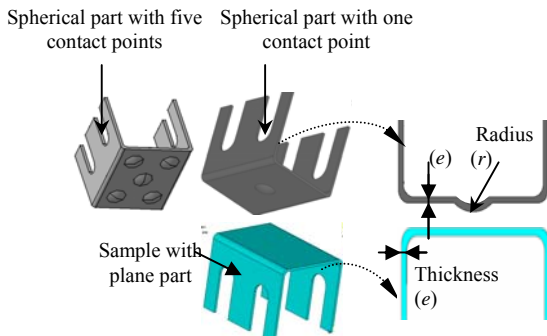


Fig. 1 U-shaped samples.

## III. MATERIAL STUDIES

The selected material C19210 of the two contact samples combines good mechanical and thermo-electrical properties. Table I and Table II show respectively thermo-electrical and mechanical properties of this copper alloys. The conductivity of the pure copper  $5.95 \cdot 10^7$  Siemens/m and is defined to be 100 % IACS at 20°C. The electrical conductivity for the C19210 material is 91 % IACS.

TABLE I  
THERMAL AND ELECTRICAL CHARACTERISTICS FOR THE USED COPPER ALLOY C19210

Copper alloy UNS Designation	Composition	Thermal conductivity (W/mK)	Electrical resistivity ( $\Omega \cdot \text{mm}$ )	Electrical conductivity (%IACS)
C19210	CuFeP	350	$1.88 \cdot 10^{-3}$	91

TABLE II  
MECHANICAL CHARACTERISTICS FOR THE USED COPPER ALLOY C19210

Copper alloy UNS Designation	Yield stress $\sigma_e$ (MPa)	Young modulus $E$ (MPa)	Vickers hardness HV	Tensile strength $\sigma_m$ (MPa)
C19210	322	$0.9 \cdot 10^5$	100-130	360

The elasto-plastic behaviour law for this material was identified by the tensile tests; this law will be implemented in the finite element code in order to simulate the mechanical behaviour of contact samples under indentation loading. Tensile test was carried out with specimens made of high-copper alloy C19210 and standardized according to the European Standard NF EN 10002-1.

Fig. 2 (a) depicts the dimensions of the used standard tensile specimen where:

$l_0$  is the initial length of tensile test specimen,  $l_0$  is calculated by the following formula :

$$l_0 = 5.65\sqrt{S_0}, S_0 = a.b \quad (1)$$

$S_0$  is the rectangular section of specimen,  $a$  is the depth of specimen and  $b$  is the width of specimen. In this study,  $a$  is equal to 2 mm,  $b$  is equal to 5 mm and  $l_0$  is equal to 17.86 mm (Fig. 2 (a)). Fig. 2 (b) shows at the end of the tensile test, the tensile specimen fractured and mounted on the clamping jaws of the tensile tester.

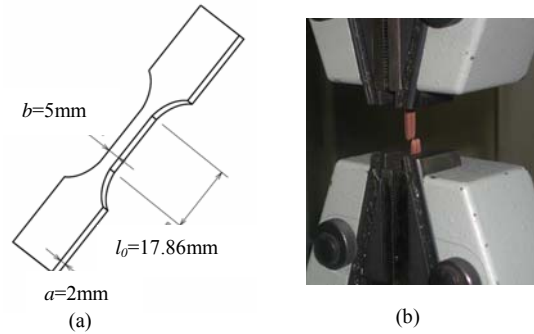


Fig. 2 Tensile testing (a) dimensions of the standard specimen and (b) fractured specimen after tensile test.

Fig. 3 presents the plotted elasto-plastic curve (stress versus strain) for the high-copper alloy C19210. The tests were carried out with a speed of  $3.3 \cdot 10^{-2}$  mm/s and with a strain rate  $\dot{\epsilon}$  of  $1.8 \cdot 10^{-3} \text{ s}^{-1}$ . The elasto-plastic law contains two parts, an elastic part and a plastic part. The elastic part is characterized by the Young modulus  $E$ , the yield stress  $\sigma_e$  (taken at 0.2 % offset strain) and the Poisson coefficient  $\nu$  which is equal to 0.33.

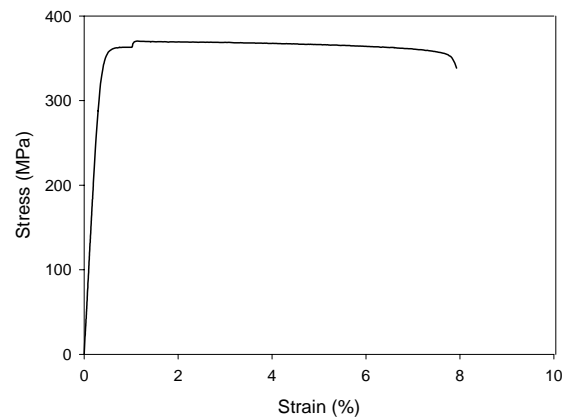


Fig. 3 Elasto-plastic behaviour law for high-copper alloy C19210. The plastic part can be characterized by the Hollomon law [20]:

$$\sigma = K \epsilon_T^n \quad (2)$$

$$\epsilon_T = \epsilon_e + \epsilon_p \quad (3)$$

$\sigma$  is the mechanical stress,  $\epsilon_T$ ,  $\epsilon_e$  and  $\epsilon_p$  are the total strain, the elastic strain and the plastic strain, respectively. Constant parameters  $n$  and  $K$  are the strain hardening exponent and the strength coefficient, respectively.  $n$  and  $K$  are calculated by an automatic fit curve based on a nonlinear regression and a power law with 2 parameters and are equal

respectively to 0.026 and 417 MPa. From (2), an expression for  $n$  value can be derived:

$$n = \frac{\varepsilon}{\sigma} \frac{d\sigma}{d\varepsilon} \quad (4)$$

#### IV. TRANSIENT THERMAL AND ELECTRICAL ANALYSIS BY FINITE ELEMENT

For three dimensional transient heat transfer, the temperature distribution  $T(x,y,z,t)$  at each point on the contact samples and function of time  $t$  is calculated by solving in Cartesian coordinates the following heat conduction governing differential equation:

$$\frac{\partial}{\partial x} \left( k \frac{\partial T}{\partial x} \right) + \frac{\partial}{\partial y} \left( k \frac{\partial T}{\partial y} \right) + \frac{\partial}{\partial z} \left( k \frac{\partial T}{\partial z} \right) + \ddot{q} = \rho C_p \frac{\partial T}{\partial t} \quad (5)$$

For isotropic material, (5) can be simplified to:

$$\alpha \left( \frac{\partial^2 T}{\partial x^2} + \frac{\partial^2 T}{\partial y^2} + \frac{\partial^2 T}{\partial z^2} \right) + \frac{\ddot{q}}{\rho C_p} = \frac{\partial T}{\partial t} \quad (6)$$

where  $k$  denotes the thermal conductivity in W/mK,  $C_p$  is the specific heat in J/kg K and  $\rho$  is the density of the material in kg/m<sup>3</sup>.  $\alpha$  is a material property called thermal diffusivity in m<sup>2</sup>/s, defined as follows:

$$\alpha = \frac{k}{\rho C_p} \quad (7)$$

$T$  is the temperature that varies with the coordinates  $x$ ,  $y$  and  $z$  as well as the time  $t$ .  $\ddot{q}$  is the Joule heat generation rate per unit volume (W/m<sup>3</sup>), this heating occurs in a conductor carrying an electric current and can be calculated by the following equation:

$$\ddot{q} = \frac{RI^2}{Vo} \quad (8)$$

where  $R$  is the sum of electrical contact resistance and electrical resistance of the two contact samples in  $\Omega$ ,  $I$  is the electric current in Ampere's,  $Vo$  is the volume of structure in m<sup>3</sup>. Using the Fourier's law, the heat conduction fluxes can be written in the  $x$ ,  $y$  and  $z$  directions as follows:

$$\begin{aligned} q_x &= -k \frac{\partial T}{\partial x} \\ q_y &= -k \frac{\partial T}{\partial y} \\ q_z &= -k \frac{\partial T}{\partial z} \end{aligned} \quad (9)$$

The heat exchange with the outside is described by the Newton's law of cooling for surface heat transfer by convection; this law is expressed as follows:

$$q_c = h(T_s - T_\infty) \quad (10)$$

where  $q_c$  is the dissipated heat flux in W/m<sup>2</sup>,  $h$  is the convective heat transfer coefficient of the ambient air in W/m<sup>2</sup>K,  $T_s$  is the unknown surface temperature of contact samples and  $T_\infty$  is the ambient temperature.

Analytical solution methods of (5) are limited to highly simplified problems in simple geometries. Numerical methods such as the finite element method permits to solve the differential equation (5) for any complex geometry subjected to any kind of thermal and electrical conditions.

Finite element formulation corresponding to the transient heat conduction governing differential equation (5) can be derived using the variational method; it is given by the following equation:

$$[C^{th}] \left( \dot{T} \right) + [K^{th}](T) = (Q) \quad (11)$$

where  $[C^{th}]$  is the thermal specific heat matrix function of the specific heat  $C_p$  and the density of the material  $\rho$ , the capacitance matrix  $[C^{th}]$  is calculated for an element (e) by the following equation:

$$[C^{th(e)}] = \rho C_p \int_{V(e)} [N_i^{(e)}]^T [N_i^{(e)}] dV \quad (12)$$

$$\dot{T}(x, y, z, t) = \frac{\partial T}{\partial t} = [N_i^{(e)}] \left( \dot{T}_i^{(e)} \right) \quad (13)$$

$S(e)$  and  $V(e)$  represent the surfaces and the volume of the element (e) respectively.

$(T) = (T(x, y, z, t))$  is the spatial and temporal vector of temperature.

$[N_i^{(e)}] = [N_i^{(e)}(x, y, z)]$ , shape functions of the element (e).

$(T_i^{(e)}) = (T_i^{(e)}(t))$  is the nodal temperature of the element (e) which depends to the time  $t$ .

$[K^{th}] = [K_{co}] + [K_h]$  is the thermal matrix and is sum of the diffusion conductivity matrix and the convection surface conductivity matrix respectively, it is calculated for an element (e) by the following equation, as in [5] and [21]:

$$\begin{aligned} [K^{th(e)}] &= \int_{V(e)} [[\bar{L}][N_i^{(e)}]]^T [\bar{D}][[\bar{L}][N_i^{(e)}]] dV + \\ &+ \int_{S(e)} h [N_i^{(e)}]^T [N_i^{(e)}] dS \end{aligned} \quad (14)$$

$$[\bar{L}] = \begin{bmatrix} \frac{\partial}{\partial x} \\ \frac{\partial}{\partial y} \\ \frac{\partial}{\partial z} \end{bmatrix}, \text{ differential operator matrix for thermal behaviour.}$$

$$[\bar{D}] = \begin{bmatrix} k(T) & 0 & 0 \\ 0 & k(T) & 0 \\ 0 & 0 & k(T) \end{bmatrix}, \text{ thermal conductivity matrix that}$$

depends to the temperature  $T$ .

$(Q)$  presents the heat flow which is composed in our study of the heat convection flow  $(Q_h)$  and the Joule heat generation flow  $(Q_Q)$  with unit W. The heat flow for an element (e) is calculated as:

$$(Q^{(e)}) = (Q_h^{(e)}) + (Q_Q^{(e)})$$

$$(Q^{(e)}) = \int_{S(e)} h T_{\infty} [N_i^{(e)}]^T dS + \int_{V(e)} q [N_i^{(e)}]^T dV \quad (15)$$

For the electrical behaviour, differential equation for electric scalar potential  $V$  is given as:

$$\frac{1}{R_{sv}} \left( \frac{\partial^2 V}{\partial x^2} + \frac{\partial^2 V}{\partial y^2} + \frac{\partial^2 V}{\partial z^2} \right) = 0 \quad (16)$$

$R_{sv}$  presents the electrical resistivity of the material.

The application of the variational principle and finite element discretization to the differential equation (16) produces for an element (e) the following system of equation:

$$[K^{v(e)}] (V_i^{(e)}) = (I_i^{(e)}) \quad (17)$$

$(I_i^{(e)})$  is the nodal electric current,  $(V_i^{(e)})$  is the nodal voltage and  $[K^{v(e)}]$  is the electrical conductivity coefficient matrix and is calculated by the following formula, as in [5] and [22]:

$$[K^{v(e)}] = \int_{V(e)} \left[ \bar{L} [N_i^{(e)}] \right]^T [\bar{C}] \left[ \bar{L} [N_i^{(e)}] \right] dV \quad (18)$$

$$[\bar{C}] = \begin{bmatrix} \frac{1}{R_{sv}(T)} & 0 & 0 \\ 0 & \frac{1}{R_{sv}(T)} & 0 \\ 0 & 0 & \frac{1}{R_{sv}(T)} \end{bmatrix}, \text{ electrical conductivity matrix.}$$

The electric scalar potential  $V$  is approximated over the element as follows:

$$V(x, y, z, t) = [N_i^{(e)}] (V_i^{(e)}(t)) \quad (19)$$

$(V_i^{(e)})$  depends to the time  $t$ , because  $(V_i^{(e)})$  depends to the temperature  $T$  in which depends on the time  $t$ .

## V. FINITE ELEMENT MODELLING

Finite element models were developed with the finite element Multiphysics code (Ansys) [5] in order to calculate the transient numerical values of contact resistance and contact temperature under indentation loading in the cases of one contact point and five contact points. The finite element calculation was run on a computer with Genuine Intel (R) Dual Core processor with a speed of 1.6 GHz and 2 Go of RAM.

### A. Indirect coupling method

Deformation of contact surface under applied contact forces, numerical contact resistance and contact temperature values were calculated basing to the indirect coupling program. This developed program is written in a macro file by a scripting language called Ansys Parametric Design Language (APDL) in order to automate the coupling between the mechanical and thermo-electrical fields. Using APDL interface it is possible to pass commands to the commercial software package, such as modelling the structure, meshing the model, applying the boundary conditions on the model, solving the problem, saving the deformed structure and changing element types and boundary conditions. Fig. 4 shows the algorithm for solving the thermoelectro-mechanical problem using the indirect coupling method.

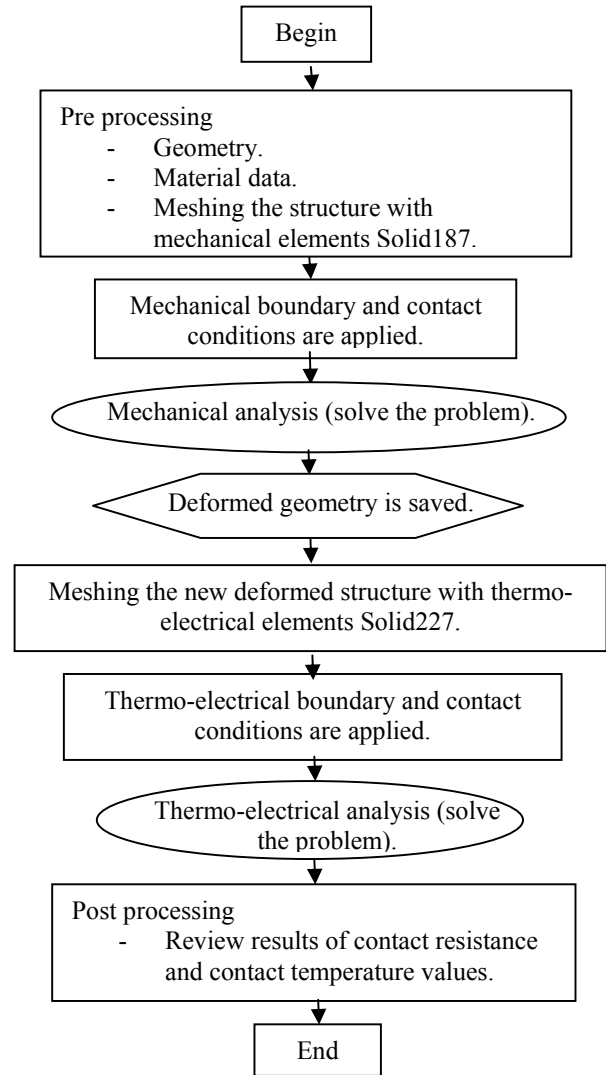


Fig. 4 Algorithm for solving thermoelectro-mechanical problem using the indirect coupling method.

The indirect coupling method (Fig. 4) begins by importing in the finite element pre-processor the geometric model of the two contact samples created by the CAD software Catia V5R19. The material properties of the two contact samples are then specified. In order to study the mechanical behaviour of contact samples under indentation loading, the previous geometric model is meshed with tetrahedral structural solid elements (Solid187-3D-10 nodes) with degrees of freedom: displacements  $U_x$ ,  $U_y$  and  $U_z$  according to the three axes  $X$ ,  $Y$  and  $Z$  respectively (Fig. 5) and with the capability to take into account the plasticity of material. Then, a mechanical boundary and contact conditions are applied to this meshing model and a nonlinear static analysis type is performed for solution in which large strain effects are included. A time associated to the applied boundary conditions of  $10^{-3}$  is specified for the end of load step and an initial integration time step size of  $10^{-6}$  is defined. After a calculus time central processing unit (CPU) of 1 hour and 7 minutes for the model with one contact point and 5 hours and 13 minutes for the model with five contact points, the deformed structure is saved and the mechanical elements (Solid187-3D-10 nodes)

are replaced by the coupled field solid elements (Solid227-3D-10 nodes) with degrees of freedom: temperature and voltage (Fig. 4). Then, a thermo-electrical boundary and contact conditions are applied to this deformed structure; these will be explained more in detail in the next paragraphs. A full transient analysis with stepped loading is performed for this thermo-electrical analysis. The numerical values of electrical contact resistance and contact temperature are calculated during a time of 1500 seconds with an initial integration time step size of 20 seconds. The thermo-electrical analysis was finished after a time CPU of 53 minutes for the model with one contact point and 2 hours and 30 minutes for the model with five contact points; then the thermo-electrical results as function of time are extracted from the post-processor of the software.

### B. Finite element meshing

Due to the symmetry of the loading or boundary conditions, materials and geometry, only a quarter of the contact samples is meshed in order to reduce modelling efforts, computational cost and CPU time. Fig. 5 gives the adopted meshes for the contact sample with spherical and plane parts. Tetrahedral structural solid h-element type with ten nodes is used to mesh the structure. This element is characterized by quadratic interpolation functions within the element and is used in order to increase the accuracy of finite element findings. A free meshing type is used to mesh the model. The model with one contact point is meshed with 28783 elements and 52364 nodes while the model with five contact points is meshed with 43471 elements and 79380 nodes. The size of the used element is 0.4 mm of edge length. Using the h-refinement method, the contact zones are refined in order to get better results. It can be seen that the result was identical even if we use a mesh with element edge length lower than 0.4 mm.

### C. Boundary conditions

The detailed coupled thermal, electrical and mechanical boundary conditions are shown in Fig. 5. For mechanical boundary conditions, a pressure corresponding to a contact force of 100 N is applied to the upper surface of the spherical contact part (Fig. 5); the lower surface of the plane part is embedded and the displacements  $U_x$ ,  $U_y$  and  $U_z$  according respectively to the three axes X, Y and Z of coordinate system are null. Due to the symmetric configuration of the contact samples, symmetry boundary conditions are applied on the symmetric surfaces of contact samples. So, a displacement constraint  $U_z = 0$  is applied on the two parallel surfaces to the plane XY, and a displacement constraint  $U_x = 0$  is applied on the two parallel surfaces to the plane YZ (see Fig. 5). For thermo-electrical boundary conditions, the upper extreme surface of the spherical part is submitted to a quarter of total electric current  $I$  which is equal to 100 A. The calculated voltage values of nodes set attached to this surface are forced to be the same during analysis for each time step. For this reason, a coupled voltage is applied to this extreme surface (Fig. 5). Zero voltage is applied to the lower extreme surface of the plane part.

To solve numerically the heat conduction equation, an appropriate boundary and initial conditions will be stated:

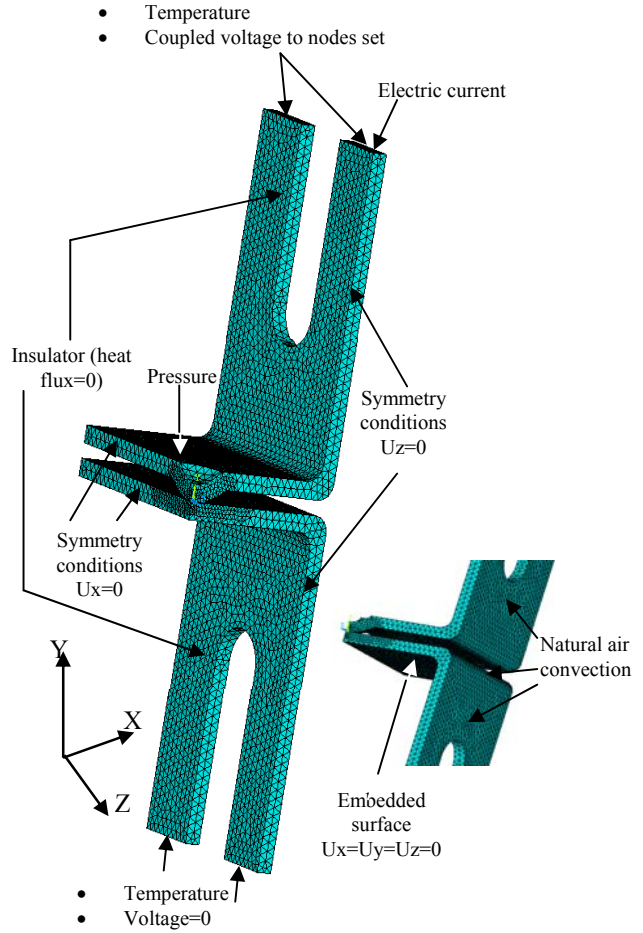


Fig. 5 Thermal, electrical and mechanical boundary conditions.

1) In the first condition, temperature function of time should be applied in the two extreme surfaces of the two contact samples, this temperature was obtained previously with the help of experimental test by Beloufa [17] (Fig. 5).

2) Second condition: The two parts of contact sample were fixed in the Teflon insulator supports. Therefore, zero heat fluxes are applied to the sample surfaces which are in contact with this insulator (Fig. 5). This second condition can be formulated mathematically as follows:

$$q_x + q_y + q_z = 0 \quad (20)$$

3) Third condition: In order to take into account the heat exchange with the outside, natural air convection with a film coefficient of  $5 \text{ W/m}^2\text{K}$  [25] and an air temperature of  $22^\circ\text{C}$  is applied to the sample surfaces exposed to the air.

This third condition is verified at any point  $(x,y,z)$  and at any instant  $t$ , it can be formulated mathematically as in [23] and [24]:

$$q_x + q_y + q_z = q_c \quad (21)$$

Substituting (9) and (10) into (21), the following equation can be obtained:

$$-k \left( \frac{\partial T}{\partial x} + \frac{\partial T}{\partial y} + \frac{\partial T}{\partial z} \right) = h (T_s - T_\infty) \quad (22)$$

4) For the fourth condition, the initial temperature distribution in the contact samples at the initial time  $t = 0$  should be specified before analysis:  $T(x, y, z, 0) = T_0 = 22^\circ\text{C}$ .

#### D. Material behaviour

To perform a mechanical analysis, nonlinear elasto-plastic law (stress versus strain) presented in Fig. 3 is used to simulate the material behaviour of high-copper alloy C19210 under indentation loading. This law is implemented as a multilinear stress-strain curve starting at the origin with positive stress and strain values. The Von Mises yield criteria of plasticity with the associated isotropic work hardening is used to determine the stress level at which the material will develop plastic strain. To perform a thermo-electrical analysis and to take into account Joule heating effects, electrical resistivity  $R_{SV}$  and thermal conductivity  $k$  must be defined; these two material properties are temperature-dependant. For example, the electrical resistivity  $R_{SV}(T)$  and thermal conductivity  $k(T)$  for the C19210 copper alloy are given by the following equations [25]:

$$R_{SV}(T) = 1.41 \cdot 10^{-26} T^2 + 7.58 \cdot 10^{-11} T + 1.71 \cdot 10^{-8} \text{ (}\Omega\text{m)} \quad (23)$$

$$k(T) = 3.46 \cdot 10^{-17} T^2 - 0.07 T + 352 \text{ (W/mK)} \quad (24)$$

Mass density  $\rho$  and specific heat  $C_p$  may be defined to take into account thermal transient effects.

#### E. Contact conditions

##### 1) Mechanical contact conditions

Contact surfaces of contact samples are meshed with a total of 411 surface to surface contact elements for the model with one contact point and 2027 surface to surface contact elements for the model with five contact points. The surface-to-surface contact model is used when contact zones are not known accurately and a significant amount of sliding is expected. In this model, one of the surfaces is called the contact surface and the other, the target surface. These two surfaces are considered deformable. Contact elements with triangular geometry located on the surfaces of 3D tetrahedral solid elements (Conta174-6 nodes) are used to mesh the spherical contact surface; target elements with triangular geometry located on the surfaces of 3D tetrahedral solid elements (Target170-6 nodes) are used to mesh the plane contact surface.

For mechanical analysis, a friction coefficient  $\mu$  equal to 0.2 is specified between the two contact surfaces in order to calculate the friction or shear stress  $\tau$  using the following Coulomb friction model:

If  $\tau < \mu P$  state is known as sticking (25)

$\tau \geq \mu P$  state is known as sliding

where  $P$  is the contact pressure. Sliding will occur if the friction stress  $\tau$  reaches a defined maximum friction stress which is equal to  $10^{20}$  MPa. The contact algorithm used is the augmented Lagrangian method which is an iterative series of penalty methods updates to find the Lagrange multipliers and it can be considered as a generalization of the Lagrange multiplier method. Contact elements use Gauss integration points as a contact detection points. The initial penetration and initial gap between contact elements are excluded. Any existing gap between contact elements is closed during analysis.

To achieve the convergence of contact problems, the initial time step size must be small enough to capture the proper

contact zone. As mentioned in the paragraph A, an initial time step size of  $10^{-6}$  has been defined for solution of contact problem.

##### 2) Thermal and electrical contact conditions

In the case of contact between solids, it is assumed that there is no temperature jump at the interface, i.e., the temperatures of the contacting surfaces are equal and there is a continuity of temperature and conservation of energy at the interface.

The heat flux  $Q$  between two contacting surfaces can be decomposed into two parts:

$$Q = Q_T + Q_E \quad (26)$$

The first term  $Q_T$  in  $\text{W/m}^2$  illustrates the conductive heat transfer between contact and target surfaces or the thermal exchanges at the interface of contact which is defined as follows:

$$Q_T = TCC (T_C - T_T) \quad (27)$$

$TCC$  is the thermal contact conductance in  $\text{W/m}^2 \text{K}$  and can be considered as the inverse of thermal contact resistance [21].

The contact and target interfaces are considered perfect, thus, the temperature of the contact interface  $T_C$  and the temperature of the target interface  $T_T$  must be the same:

$$T_C(x, y, z, t) = T_T(x, y, z, t) \quad (28)$$

To verify the last condition (28), the value of  $TCC$  must be taken very high; a reasonable value of  $10^6 \text{ W/m}^2 \text{K}$  is given to the thermal contact conductance  $TCC$ . It is interesting to note that the numerical calculus was not converged when a value of  $TCC$  higher than  $10^6 \text{ W/m}^2 \text{K}$  has been used. The second term  $Q_E$  in  $\text{W/m}^2$  of the previous equation (26) represents the thermal power dissipated by the Joule effect at the interface or the heat flux at the interface due to electric current,  $Q_E$  can be expressed as follows:

$$Q_E = J (V_C - V_T) = ECC (V_C - V_T)^2 \quad (29)$$

where  $J$  is the electrical current density in  $\text{A/m}^2$ ,  $V_C$  and  $V_T$  are the electric potential of the contact interface and target interface respectively in Volt,  $ECC$  is the electrical contact conductance in  $\Omega^{-1}\text{m}^{-2}$  or Siemens/ $\text{m}^2$  and can be considered as the inverse of electrical contact resistance per unit area. As in the thermal contact, for a perfect electric contact and target interfaces, the voltage of the contact interface  $V_C$  and the voltage of the target interface  $V_T$  must be the same, thus:

$$V_C(x, y, z, t) = V_T(x, y, z, t) \quad (30)$$

The previous condition (30) is verified when the potential difference approaches toward zero. Consequently, the value of  $ECC$  must be taken very high; a value of  $10^{14} \Omega^{-1}\text{m}^{-2}$  is given to the electrical contact conductance  $ECC$  [26] and [27] which is the maximum value accepted by the used finite element commercial code in order to minimize the voltage drop between the target and contact surfaces.

Finally,  $TCC$  and  $ECC$  mainly depend on the roughness of the contact surfaces, contact area and on the pressure force of both bodies. However, a theoretical determination of these coefficients is extremely difficult. For this reason, the contact and target interfaces are considered perfect.

## VI. NUMERICAL RESULTS AND DISCUSSIONS

For mechanical analysis, contact, material and geometric non-linearities require an iterative full Newton Raphson method to be used with the sparse matrix solver (direct solver) for solving nonlinear systems of equations. In this approach, the applied load is subdivided into a series of load increments which can be applied over several load steps. The program checked the convergence of the iterative solution by using a force criterion, i.e. the solution is achieved when the calculated force convergence norm does not exceed the defined force criterion. The maximum number of equilibrium iterations allowed for each substep and for nonlinear analysis is 25. For thermo-electrical analysis, contact and material properties which are temperature-dependant require also the use of full Newton-Raphson method with sparse solver to solve the thermal transient problem. The program checked the convergence of the iterative solution by using a heat flow criterion, i.e. the solution is achieved when the calculated heat flow convergence norm does not exceed the defined heat flow criterion. The advantage of the developed finite element model is the prediction of the electrical contact resistance without making the experimental test and the calculation of the temperature of contact surfaces which is impossible to measure it by our experimental means. Fig. 6 (a) and (b) show for the two models (with one contact point and five contact points) the numerical curves of contact temperature and electrical contact resistance variations during 1500 seconds. The temperature varies exponentially and increases over time until the equilibrium state when the time reaches approximately 1500 seconds with an equilibrium contact temperature of 41.23 °C for the model with one contact point and is higher than the one obtained for five contact points which is equal to 32.05 °C. The electrical contact resistance increases exponentially with time because the resistivity increases with the increase of contact temperature. Also, we remark that the electrical contact resistance for one contact point is higher than the one obtained for five contact points. Fig. 7 shows at the end of analysis a comparison between the Von Mises stress, temperature and electrical resistance distributions on the half of contact samples for the model with five contact points and for the model with one contact point. The applied indentation force  $F_c$  is 100 N and the applied current  $I$  is 100 A. However, the applied contact force is high, thus leads to obtain a large contact zones and a lower electrical contact resistance and contact temperature. Electrical contact resistance decreases inversely to the applied load [3], [28]. Fig. 7 shows that the maximum Von Mises stress is localized near to the contact zones for the two model, the maximum Von Mises stress for the model with one contact point ( $\sigma_{VM}^{Max} = 351$  MPa) is slightly higher than the yield stress of copper alloy C19210 ( $\sigma_e = 322$  MPa) which confirms the presence of a little plastic strain near to the contact zone (Fig. 7). The maximum Von Mises stress for the model with five contact points ( $\sigma_{VM}^{Max} = 177$  MPa) is very lower than the maximum stress for the model with one contact point ( $\sigma_{VM}^{Max} = 351$  MPa) and very lower also than the yield stress of copper

alloy C19210 ( $\sigma_e = 322$  MPa) (Fig. 7). This leads to increase the life time of contact samples with five contact points.

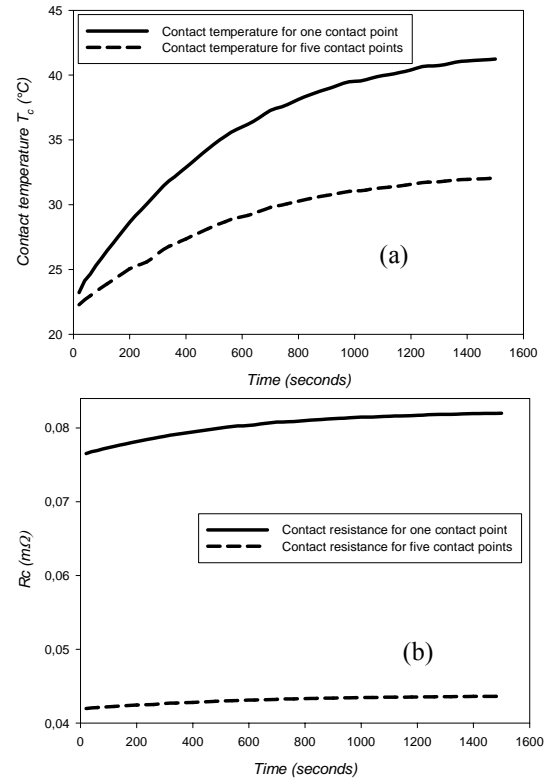


Fig. 6 Transient numerical variation of (a) contact temperature (b) and electrical contact resistance.

At 1500 s, electrical contact resistance for the model with five contact points is reduced by 47 % with report to the electrical contact resistance obtained for the model with one contact point (0.082mΩ) (Fig. 7). This induces the temperature to decrease due to a generation of lower Joule heat in the contact zones. This temperature is reduced for the model with five contact points by 22% with report to the calculated temperature for the model with one contact point (41.23 °C) (Fig. 7). Finally, the finite element model with five contact points presents several gains: contact resistance, contact temperature and maximum Von Mises stress which is more interesting for the connector designers.

## VII. CONCLUSION

Minimisation of volume design, electrical contact resistance, contact temperature and maximum stress of contact samples made of recent high-copper alloys under different contact forces and electric currents was studied in this work with the help of experimental and numerical means. Using an indirect coupling method, a finite element analysis of mechanical stress and transient electrical contact resistance and contact temperature of contact samples (with one and five contact points) made of C19210 copper alloy has been carried out with an applied contact force of 100 N and an applied electric current of 100 A.

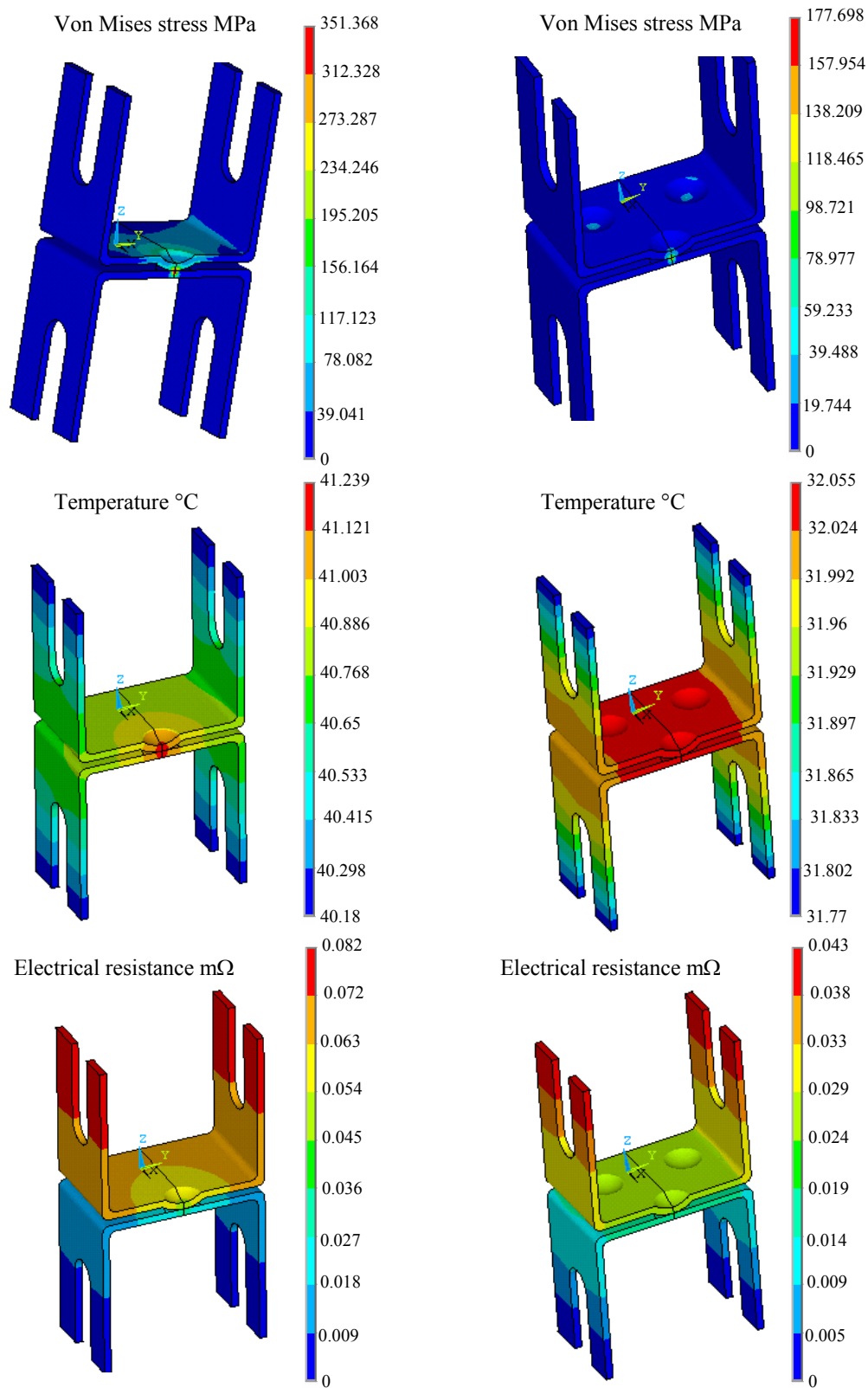


Fig. 7 Comparison results between the model with one contact point and the model with five contact points

The model developed in this study is beneficial in understanding the coupled mechanical, thermal and electrical behaviour of the electrical contact, and can be applied to predict the contact resistance and contact temperature without making the experimental test.

In this study, a comparison has been made between the results of the model with one contact point and the results of the model with five contact points. The model with five contact points presents many advantages: minimization of contact resistance without changing the volume, minimisation of contact temperature and maximum Von Mises stress which is also lower than the yield stress of the material C19210. This leads to decrease the connector cost and to increase the life time of contact samples. In this work, the result quality in terms of accuracy and efficiency are tested and discussed with different finite element analysis models.

## REFERENCES

- [1] R. S. Timsit, "On the evaluation of contact temperature from potential-drop measurements," *IEEE Transactions on Components, Hybrids, and Manufacturing Technology*, vol. 6, no. 1, pp. 115–121, March 1983.
- [2] A. Beloufa, "Conduction degradation by fretting corrosion phenomena for contact samples made of high-copper alloys," *Tribology International*, vol. 43, no. 11, pp. 2110–2119, November 2010.
- [3] R. El Abdi, A. Beloufa, N. Benjemaa, "Contact resistance study of high-copper alloys used in power automotive connectors," *Journal of Automobile Engineering Part D*, vol. 222, no. 8, pp. 1375–1383, August 2008.
- [4] A. Beloufa, "Investigation on contact surface damage of automotive connector by fretting corrosion," in *2010 3<sup>rd</sup> Int. Conf. on Tribology and Design*, Algarve, Portugal, pp. 141–154.
- [5] Ansys, *Release 10.0* (Ansys Inc. Canonsburg Southpointe, PA 15317, USA, 2007). Available: <http://www.ansys.com>
- [6] H. Akbulut, "On optimization of a car rim using finite element method," *Finite Elements in Analysis and Design*, vol. 39, no. 5–6, pp. 433–443, March 2003.
- [7] W. Annicchiarico, M. Cerrolaza, "Structural shape optimization 3D finite-element models based on genetic algorithms and geometric modelling," *Finite Elements in Analysis and Design*, vol. 37, no. 5, pp. 403–415, May 2001.
- [8] G. Corriveau, R. Guilbault, A. Tahan, "Genetic algorithms and finite element coupling for mechanical optimization," *Advances in Engineering Software*, vol. 41, no. 3, pp. 422–426, March 2010.
- [9] A. R. Khoei, Sh. Keshavarz, S. O. R. Biabanaki, "Optimal design of powder compaction processes via genetic algorithm technique," *Finite Elements in Analysis and Design*, vol. 46, no. 10, pp. 843–861, October 2010.
- [10] Z. Wu, "An efficient approach for shape optimization of components," *International Journal of Mechanical Sciences*, vol. 47, no. 100, pp. 1595–1610, October 2005.
- [11] W. Song, A. Keane, J. Rees, A. Bhaskar, S. Bagnall, "Turbine blade fir-tree root design optimisation using intelligent CAD and finite element analysis," *Computers and Structures*, vol. 80, no. 24, pp. 1853–1867, September 2002.
- [12] D. Hilding, B. Torstenfelt, A. Klarbing, "A computational methodology for shape optimization of structures in frictionless contact," *Computer methods in applied mechanics and engineering*, vol. 190, no. 31, pp. 4043–4060, April 2001.
- [13] J. T. Chiu, D. Y. Chang, "A new probe design combining finite element method and optimization used for vertical probe card in wafer probing," *Precision Engineering*, vol. 33, no. 4, pp. 395–401, October 2009.
- [14] C. H. Cheng, C. K. Chan, G. J. Lai, "Optimal design of Al/Si bimorph electro-thermal microactuator by integrating finite-element code with optimization method," *Sensors and Actuators*, vol. 151, no. 1, pp. 53–63, April 2009.
- [15] A. Plankensteiner, A. Leuprecht, B. Schedler, K. H. Scheiber, H. Greuner, "Finite element based design optimization of WENDELSTEIN 7-X divertor components under high heat flux loading," *Fusion Engineering and Design*, vol. 82, no. 15–24, pp. 1813–1819, October 2007.
- [16] J. J. del Coz Diaz, P. J. Garcia Nieto, J. L. Suarez Sierra, C. Betegon Biempica, "Nonlinear thermal optimization of external light concrete multi-holed brick walls by the finite element method," *International Journal of Heat and Mass Transfer*, vol. 51, no. 7–8, pp. 1530–1541, April 2008.
- [17] A. Beloufa, "Influence of shapes, contact forces and high copper alloys on the contact resistance and temperature," in *2009 Proc. EMESEG Int. Conf.*, Rodos Island, Greece, pp. 139–144.
- [18] R. Zauter, D. V. Kudashov, "Precipitation hardened high-copper alloys for connector pins made of wire," in *2006 Int. Conf. on Electrical Contacts*, Sandai, Japan, pp. 257–261.
- [19] Company Weiland specialist in copper and copper alloys, Available: <http://www.wieland.de/internet/index.jsp>
- [20] J. H. Hollomon, "Tensile deformation," *Transactions of the American Institute of Mining and Metallurgical Engineers*, vol. 162, pp. 268–290, 1945.
- [21] J. M. Bergheau, R. Fortunier, "Finite element simulation of heat transfer," Ed. Hoboken and London: ISTE Ltd and John Wiley & Sons, 2008.
- [22] H. Zhigang, W. Yuanxun, L. Chunzhi, C. Chuanyao, "A multi-coupled finite element analysis of resistance spot welding process," *Acta Mechanica Sinica*, vol. 19, no. 1, pp. 86–94, March 2006.
- [23] R. W. Lewis, P. Nithiarasu, K. N. Seetharamu, "Fundamentals of the finite element method for heat and fluid flow," Ed. John Wiley & Sons, 2004.
- [24] A. Bhatti, "Fundamental finite element analysis and applications," Ed. Hoboken, New Jersey: John Wiley & Sons, 2005.
- [25] Handbook of chemistry and physics, Ed. New York: CRC Press, 2005.
- [26] P. Cavaliere, V. Dattoma, F. W. Panella, "Numerical analysis of multipoint CDW welding process on stainless AISI304 steel bars," *Computational Materials Science*, vol. 46, no. 4, pp. 1109–1118, October 2009.
- [27] X. Lai, D. Liu, L. Peng, J. Ni, "A mechanical–electrical finite element method model for predicting contact resistance between bipolar plate and gas diffusion layer in PEM fuel cells," *Journal of Power Sources*, vol. 182, no. 1, pp. 153–159, July 2008.
- [28] R. Holm, "Electric contacts: theory and applications," 4th ed., Ed. Berlin, Springer Verlag, 1999.

**A. Beloufa** Mechanical engineer from the University of Tlemcen (Algeria) in 2004, he received a Master of research in mechanical engineering degree from the University Paul Sabatier Toulouse (France) in 2005. He received a Ph.D. degree in mechanic from the University of Rennes1 (France) in 2008. His current research interests include numerical and experimental simulation of power electrical contacts, thermoelectro-mechanical simulation of electrical contact, experimental analyses of contact surfaces etc. He has published about 9 papers on electrical contact phenomena in many international journals, proceedings and books. At present, he works as professor in the ENSI of Bourges in France.